

Hydriding kinetics of LaNi₅ using Nucleation-growth and Diffusion Models

J. Payá^{1,*}, A. Freni², J.M. Corberán¹ and V. Compañ³

¹Universidad Politécnica de Valencia, Instituto de Ingeniería Energética, Valencia, Spain

²C.N.R. – Institute for Advanced Technologies ITAE, Messina, Italy

³Universidad Politécnica de Valencia, Departamento de Termodinámica Aplicada, Valencia, Spain

Received: December 29, 2011, Accepted: February 09, 2012, Available online: February 22, 2012

Abstract: In this paper, the hydriding kinetics of a LaNi₅ alloy have been measured with a thermo-gravimetric system. The rate controlling steps have been analyzed. In the $\alpha+\beta$ phase, a first order Johnson-Mehl-Avrami model provides a good agreement with the measurements. In the β phase, the previous approach shows that the reaction becomes progressively controlled by the diffusion of hydrogen atoms through the hydride. In order to support this hypothesis, a Crank-Nicholson diffusion model has also been applied and achieved good results. The results show that the transition in the rate controlling mechanism takes place before the static pressure-composition isotherms are reached.

Keywords: Metal hydride; LaNi₅; Kinetics; Diffusion model

1. INTRODUCTION

The study of hydrogen storage remains a great challenge for the development of fuel cell technologies such as SOFC (Solid Oxide Fuel Cells) and PEMFC (Polymer Electrolyte Membrane Fuel Cells). Due to safety problems encountered with traditional techniques (cryogenic or compressed gas), the use of solid-state materials with higher reversibility on the absorption (or desorption) of hydrogen is promising, and has been actually a matter of research [1]. Furthermore, fast hydriding/dehydriding kinetics are necessary for some applications, in particular for metal hydride fuel cells or for coupled metal hydride tanks and fuel cell systems [2]. For these reasons many experimental and theoretical works have been developed with the aim to understand the controlling mechanism of the hydrogen absorption and desorption kinetics [3].

The hydriding reaction takes place in 5 sequential steps [4]:

- (i) Physisorption (or physical adsorption) of hydrogen molecules
- (ii) Chemisorption (or chemical adsorption); dissociation of hydrogen molecules into atoms in the surface of the hydride

- (iii) Penetration of the hydrogen atoms through the surface layer into the bulk
- (iv) Diffusion of the hydrogen atoms through the hydride
- (v) Hydride formation (nucleation and growth)

The kinetics of hydrogen sorption in activated LaNi₅ alloys was investigated by Boser [5] and Tanaka et al. [6] by means of pressure variation in a constant volumetric equipment and Miyamoto et al. [7] using a mass flow meter under constant pressure. In these papers the authors proposed an analytical expression of the kinetic rate and conclude that: i) the effect of the hydrogen pressure on the hydriding reaction rate can be expressed as $\ln(P/P_{eq})$, ii) the mobility is a thermally activated process and can be represented by an Arrhenius behaviour, iii) the rate-controlling step in the plateau range of LaNi₅ is assumed to be the chemical reaction at the interface between the unreacted core of the particle and the hydride.

Although a detailed model of the complete hydriding reaction would require the modelling of each intermediate process [8], in practice there is often a limiting step which controls the reaction, while the other steps are in equilibrium. Hence, the modelling of the rate controlling reaction may be sufficient to predict the overall reaction rate of a metal hydride system.

*To whom correspondence should be addressed: Email: jorpaher@iie.upv.es
Phone: +34 963879910, Fax: +34 963877272

NOMENCLATURE

P	Pressure, bar
ΔH	Enthalpy of formation, J mol ⁻¹
ΔS	Entropy of formation, J mol ⁻¹ K ⁻¹
R	Universal gas constant, J mol ⁻¹ K ⁻¹
T	Temperature, K
fs	Slope in the $\alpha+\beta$ phase-region
w	Metal hydride concentration, g MH/g alloy (%)
m	Mass, g
f	Reacted fraction as expressed in Eq. (1)
k	Reaction rate, s ⁻¹
n	Reaction order
D	Diffusion coefficient, cm ² s ⁻¹
r ₀	Mean particle radius, cm
t	Time, s
φ	Temperature and pressure dependent function in Eq. (6)
NRMSE	Normalised root mean square error in Eq. (11)
p	Number of measurements for each tested pressure and isotherm
CV	Calculated variable in Eq. (11)
MV	Measured variable in Eq. (11)
Subscripts	
MH	Metal hydride
α	α single phase region in the P-C-T curves
β	β single phase region in the P-C-T curves
$\alpha+\beta$	$\alpha+\beta$ phase region in the P-C-T curves
mid	Middle of the $\alpha+\beta$ phase region
init	Initial conditions
∞	Final conditions
eq	Equilibrium in the two-phase region
s	Sample of alloy in the suspension balance
0	Reference conditions (hydrogen pressure P ₀ =1 bar)

In the literature different models based on the rate controlling mechanisms have been proposed but the most extended model is the Johnson-Mehl-Avrami model (JMA) which has been validated with different sorption experimental data, not only for LaNi₅ [9,10] but also for other alloys [11-14]. Nevertheless, in the β phase, where the alloys often present a diffusion-controlled reaction [14,15], only a few diffusion models have been applied [4,16,17].

In this work we have first analyzed the sorption curves by applying a JMA model. As the reaction becomes progressively controlled by the diffusion of hydrogen atoms through the hydride, we have then applied the Crank-Nicholson (CN) diffusion model [18] for all LaNi₅ hydriding tests. From these models the reaction rate constant and the hydrogen diffusion coefficient have been correlated accurately with the temperature and pressure, hereby providing a simple tool for the prediction of the absorption curves under

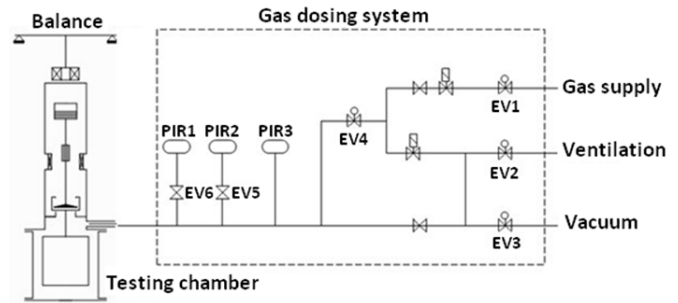


Figure 1. Scheme of the thermo-gravimetric system



Figure 2. Photograph of the measuring chamber and balance (left) and gas dosing system (right)

different temperature and pressure conditions.

Furthermore, a new aspect which has been introduced is the comparison between the static and the dynamic pressure-composition isotherms of LaNi₅. Recently, this approach has been applied for mischmetal-based alloys [19,20].

2. EXPERIMENTAL

2.1. Description of the set-up and measurement procedure

Figure 1 and Figure 2 show the layout of the thermo-gravimetric system, which may be divided into two parts:

1) A magnetic suspension balance (on the left-hand side of Fig. 1), consisting of a measuring cell with a sample holder which is magnetically coupled with an external balance. With this set-up, high pressures and/or temperature conditions (up to 20 bar at 500°C or up to 150 bar at 250°C) can be tested without damaging the weight sensor, even using corrosive or dangerous gases. The main technical characteristics of the balance are the following: resolution 0.01

mg, reproducibility +/- 0.02 mg, uncertainty <0.002%, maximum sample load capacity 20 g. The measuring cell is equipped with two heating devices: a direct electric system for the heating of the sample and a thermostated jacket for accurate measurement at temperatures from 20°C to 150°C (temperature control accuracy +/- 0.01°C).

2) The gas supply system (on the right hand side of Figure 1) equipped with pneumatic shut-off valves that allow controlling the static gas pressure around the tested sorption material. The mentioned device also helps discharge the pressure of the measuring cell (ventilation) and evacuates the cell for initial degassing (evacuation with a high vacuum turbo/drag hybrid pump). Several pressure sensors (pressure ranges 1.7, 20 and 200 bar, reproducibility +/- 0.04% to +/- 0.1%) and Pt100-type thermo-resistances are employed and the measurements are monitored throughout the sorption reaction with a PC.

The electrical heating and the operation of the gas supply system are controlled electronically. An acquisition data system and a management software are used to perform the measurements either manually or automatically.

2.2. Samples preparation

The measurement of the sorption kinetics requires a preliminary preparation of the sample. Once this was done, the sorption kinetics or the static P-C-T curves were measured.

Before starting the measurement, the LaNi₅ sample (Ergenics Inc., Hy-Stor alloy 205®) was pre-treated in order to remove all gases from the measuring cell. This was realised by evacuating the system until vacuum conditions (10⁻⁴ mbar).

The sample was first activated by applying ten consecutive absorption/desorption cycles at ambient temperature. At the end of the activation process, preliminary cycles were carried out in order to verify the stability of the sample. These preliminary tests were carried out at ambient temperature with consecutive hydriding and dehydriding at 5 bar and 1 bar respectively. After these verifications, the sample was evacuated again.

2.3. Thermo-gravimetric sorption measurements

The P-C-T equilibrium curves and the kinetic measurements were performed in the temperature range (T) 20-60°C and under hydrogen pressures (P) 1-10 bar.

In order to obtain the static P-C-T curves, the hydrogen pressure around the sample (1.0 g of commercial LaNi₅) was gradually increased at constant temperature. The absorbed mass of hydrogen was measured as the increase of the sample weight m_s . The required time to reach equilibrium was around 0.2 to 2 hours depending on the pressure and temperature conditions. The hydrogen uptake has been calculated as $(m_s(t) - m_{s,init})/m_{s,init} \times 100$ following the common nomenclature wt.% ($[H]/[M+H] \times 100$) [21]. $m_{s,init}$ is the initial sample mass of the LaNi₅ alloy in equilibrium with the hydrogen gas at P_{init} (0.97 bar in the thermo-gravimetric measurements).

The sorption kinetic measurements were performed by applying stepwise changes of pressure ΔP to the measuring cell. A similar amount of LaNi₅ sample (around 1 g) was used in order to reduce thermal effects. For all the hydriding reactions, the temperature increase was held below 1.5 K. The heat produced during the sorption process was efficiently dissipated owing to the high heat ca-

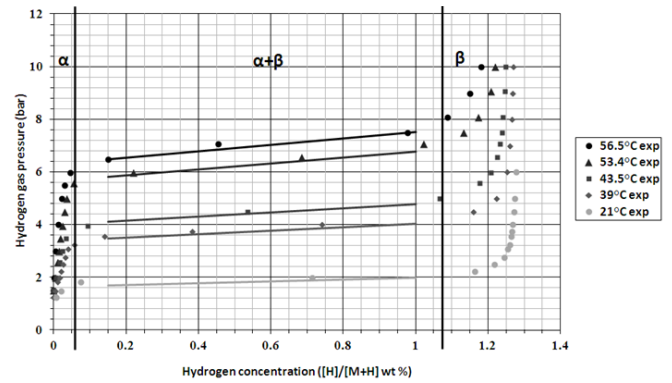


Figure 3. Equilibrium P-C-T characterization of LaNi₅

capacity of the measuring cell. The increasing sample mass was measured during the hydrogen sorption tests as a function of time at fixed temperature and pressure conditions. The measured data were properly corrected taking into account the buoyancy effect as described in [22].

2.4. Tested material

The first step in the study was to characterize the static P-C-T behaviour of the LaNi₅ alloy. Figure 3 shows the equilibrium pressures for different isotherms, as a function of the hydrogen concentration. Each experimental data point corresponds to the saturation at constant temperature of a fully dehydrated sample. The isotherms indicate three different regions. 1) α -phase region corresponding to a solid solution, 2) β -phase region indicating a hydride phase with randomly distributed vacancies and 3) the $\alpha+\beta$ -phase where the hydrogen saturated alloy and hydride phase coexist. The points of the intersection of the plateau region with the steeply sloping portions for each isotherm define the phase transitions: $\alpha \rightarrow \alpha+\beta$ and $\alpha+\beta \rightarrow \beta$.

As in previous work [23,24], the behaviour of the alloys in the two-phase region ($\alpha+\beta$, concentration range from 0.15% to 1%) was modelled with the modified Van't Hoff equation Eq. (1).

$$\ln \frac{P_{eq}}{P_0} = \frac{\Delta H}{R \cdot T} - \frac{\Delta S}{R} + fs \cdot (w - w_{mid}) \quad (1)$$

where P_{eq} is the hydrogen equilibrium pressure in the plateau region, P_0 is the reference pressure (1 atm), ΔH and ΔS are the enthalpy and entropy of formation of the hydride, respectively, R the universal gas constant, T the absolute temperature of the experiment. The third term in Eq. (1) stands for the increase of pressure in the $\alpha+\beta$ or "plateau" region, where fs is the slope in the $\alpha+\beta$ phase-region and w and w_{mid} are the hydrogen concentration (g MH/g alloy expressed in percentage (%)) in each point and in the middle of the phase region, respectively [25].

Table 1. Parameters of the P-C-T equilibrium correlation

ΔH	-30310 ± 150	J mol ⁻¹
ΔS	-108.1 ± 0.5	J mol ⁻¹ K ⁻¹
fs	0.176	-
w_{mid}	0.575	g MH/g alloy (%)
R^2 coefficient	0.994	-

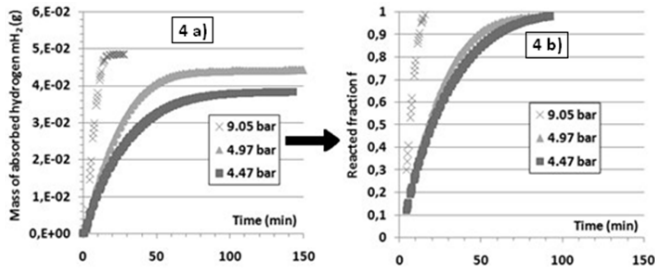


Figure 4. Measured data and filtering method at 43°C

The adjustment of the P-C isotherms (Fig. 3) to Eq.(1) provides the calculation of the thermodynamic parameters which are given in Table 1. The correlation coefficient is 0.994 indicating a good agreement between the modified Van't Hoff equation and the real behaviour of the tested sample.

3. SORPTION MODELS

In this section, two different models are described to predict the absorption reaction rate. The gravimetric sorption method involves measurements of the hydrogen mass versus time which has been absorbed owing to the reaction with the metal lattice. Typical time variations of the amount of hydrogen mass absorbed for different pressures are given in figure (4-left). As each temperature and pressure leads to a different hydrogen concentration depending on the position in the static P-C-T diagrams (Figure 3), in order to compare different P-T conditions, it is very useful to calculate the reacted fraction, as in Eq. (2):

$$f(t) = \frac{m_{H_2}(t)}{m_{H_2,\infty}} = \frac{m_s(t) - m_{s,init}}{m_{s,\infty} - m_{s,init}} \quad (2)$$

where $m_s(t)$ and $m_{s,\infty}$ are the mass of the sample at time t and at equilibrium, respectively. Typical time variations of the reacted fraction, $f(t)$, versus time are given in Figure (4-right) for the tested LaNi₅ alloy. The plots of figure 4 show the influence of the pressure on the hydriding kinetics of the activated LaNi₅ and how the experimental data has been treated (the experimental points where the reacted fraction is greater than 98% have been discarded). The evolution of the reacted fraction may be obtained for each tested pressure and temperature. After the initial induction period, the reacted fraction increases exponentially until the final concentration is achieved, as given in the static P-C-T curves (Figure 3).

A close inspection of figure 4 shows that for low pressures the time to reach the saturated state is around 70 to 80 minutes, whereas at 9.05 bar, this time is reduced four times, down to 20 minutes. The intrinsic reaction kinetics, or the hydrogen absorption rate, is relatively slow because of the small pressure gradient. In this work, a small difference has been applied between the supply pressure and the equilibrium pressure in the middle of the plateau in order to capture better the kinetics in the $\alpha+\beta$ phase region. The two mechanisms involved in Figure 4 can be described as: 1) An initial stage of the reaction where the hydrogen is dissolved in the surface region of the alloy similar to an induction period until the reaction commences. This process starts slowly and the hydride nucleation starts afterwards. 2) The growth of the hydride nuclei

and the formation of the hydride layer [13,26,27].

3.1. Johnson-Mehl Avrami (JMA) nucleation and growth model

The experimentally obtained kinetics can be described by the Johnson-Mehl-Avrami model (JMA) [11-13,28]. This model is based on the assumption of an exponential evolution of the reacted fraction with the following equation:

$$f(t) = 1 - \exp(-kt^n) \quad (3)$$

where k is the reaction rate constant and n is the Avrami exponent or the reaction order. Equation (3) may be rewritten as follows:

$$\ln[-\ln(1-f)] = n \cdot \ln t + \ln k \quad (4)$$

Thus, if the kinetics behave according to the JMA model, a plot of $\ln[-\ln(1-f)]$ against $\ln t$ (time) at a given temperature should reveal a linear tendency. The slope of the linear regression gives the reaction order n .

In order to correlate the reaction rate constant with the temperature and pressure conditions, $k(P,T)$, a semi-empirical approach has been used, by correlating the pressure and temperature dependence with the polynomial expression which is given in Eq. (5):

$$k(P,T) = k_0 + k_1 \cdot \varphi(P,T) + k_2 \cdot \varphi(P,T)^2 \quad (5)$$

The function $\varphi(P,T)$ is calculated with Eq. (6), where the weight of the tank pressure and equilibrium pressure is described by a logarithmic expression, in agreement with other authors [29-33]:

$$\varphi(p,T) = \ln\left(\frac{P_\infty}{P_{eq,mid}}\right) \quad (6)$$

The previous function $\varphi(P,T)$ helps $\varphi(P,T)$ correlate the reaction rate with both the tank pressure (P_∞) and the temperature (which defines the equilibrium pressure $P_{eq,mid}(T)$) by means of the modified Van't Hoff Eq. (1).

3.2. Crank-Nicholson (CN) diffusion model

From the observations of the reaction rate in the β phase we have calculated the hydrogen diffusion coefficient through the metal hydride lattice using the CN diffusion model. We have hereby assumed that the diffusion coefficient is independent on the instantaneous metal hydride concentration [34].

The hydrogen diffusion takes place from the surface of the particles (mean radius r_0) towards the centre. Taking into account that the expression of the diffusion within a sphere is given by [17]:

$$f(t) = 1 - \frac{6}{\pi^2} \sum_{m=0}^{\infty} \frac{1}{(2m+1)^2} \exp(-D(2m+1)^2 \pi^2 \frac{t}{r_0^2}) \quad (7)$$

where D is the diffusion coefficient, r_0 the average particle radius and t is the time, and for high time values, only the first term of the series is significant [18,34]. The solution of Eq. (7) reduces itself to a fairly simple expression (8).

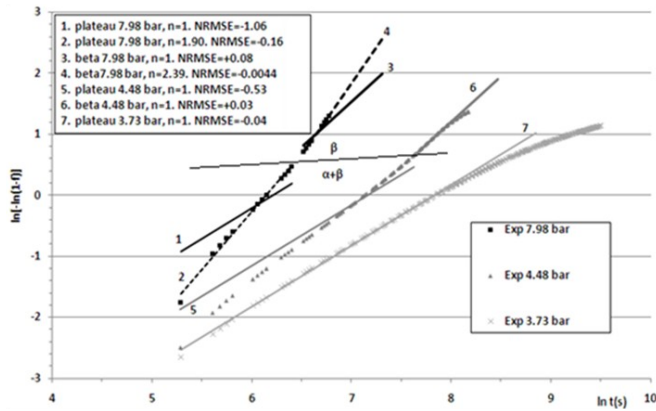


Figure 5. JMA model adjustment at 39°C ($n_{\alpha+\beta}=1$; $n_{\beta}=1.5$)

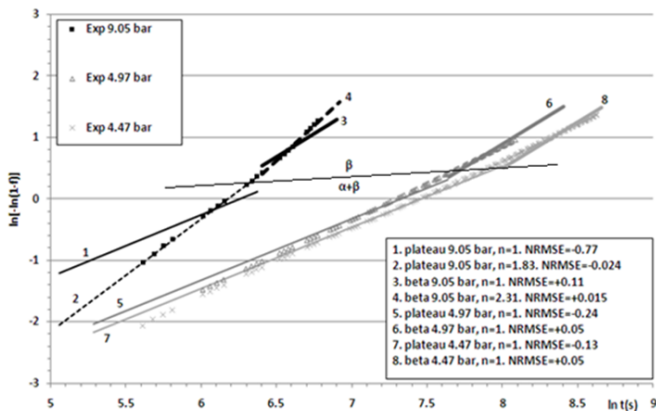


Figure 6. JMA model adjustment at 43°C ($n_{\alpha+\beta}=1$; $n_{\beta}=1.5$)

$$\ln[1-f] = \ln\left[\frac{6}{\pi^2}\right] - \frac{D}{r_o^2} \cdot \pi^2 \cdot t \quad (8)$$

As for the reaction rate constant, the diffusion coefficient also depends on the temperature and pressure conditions. Thus we have assumed the same functional expression $\varphi(P,T)$:

$$\frac{D}{L^2}(p,T) = D_0 + D_1 \cdot \varphi(P,T) \quad (9)$$

where D_0 represents the overall diffusion rate when the applied pressure is equal to the equilibrium pressure in the middle of the two-phase region $P_{eq,mid}$. D_1 accounts for the impact of the supply pressure on the hydrogen diffusion process, for supply pressures other than the plateau pressure $P_{eq,mid}$. In this work, a linear relationship between the diffusion coefficient with the function $\varphi(P,T)$ has provided good results, as will be presented in subsection 4.2.

4. RESULTS AND DISCUSSION

In Figs. 5 to 11, the JMA and the CN models have been fitted to the experimental absorption curves. The quality of the fitting is shown by means of the NRMSE statistical parameter (Normalised

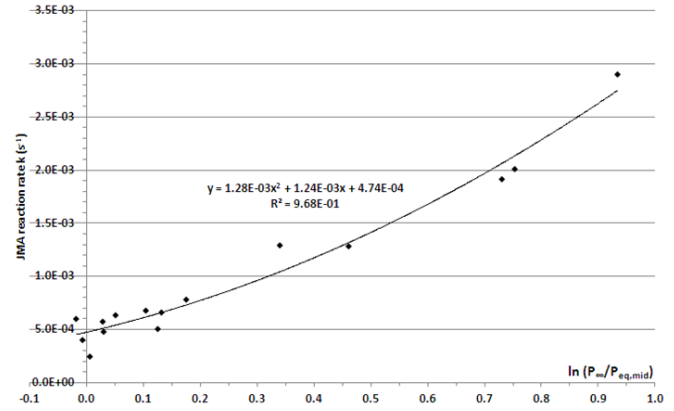


Figure 7. Reaction rate pressure dependence in the $\alpha+\beta$ phase

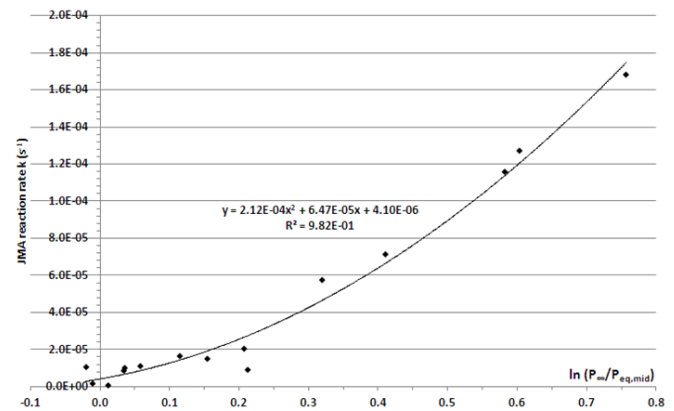


Figure 8. Reaction rate pressure dependence in the β phase

Root Mean Square Error), which is defined as in Eq. (10):

$$NRMSE = \frac{\left(\frac{1}{p} \cdot \sum_{i=1}^p (CV_i - MV_i)^2\right)^{\frac{1}{2}}}{\frac{1}{p} \cdot \sum_{i=1}^p MV_i} \quad (10)$$

where p is the number of measurements, CV_i and MV_i are the calculated and measured variables respectively. The terms which have been compared are $CV_i = \ln[-\ln(1-f_i)]$ and $MV_i = \ln[-\ln(1-f_{exp,i})]$. The calculated values of CV_i are obtained by applying the JMA model (Eq. (4)) or with $\ln[-\ln(1-f)]$ for the CN method.

NRMSE values close to zero indicate that the mean square error is small and that the quality of the fitting is good. For some absorption curves, the NRMSE is negative because the mean measurement term $MV_i = \ln[-\ln(1-f_{exp,i})]$ is negative, particularly when the reacted fractions are below 64%.

4.1. JMA model

In Figures 5 to 8, the JMA model has been adjusted to the measured hydriding curves. 5 different isotherms have been studied (22°C, 39°C, 43°C, 53°C, 57°C), each of them under three different pressures ranging from 2 bar to 10 bar. As may be inferred from Figure 3, for the isotherm at 39°C a minimum of 4 bar is necessary to reach the β phase. Thus, for an applied pressure of 3.73 bar in

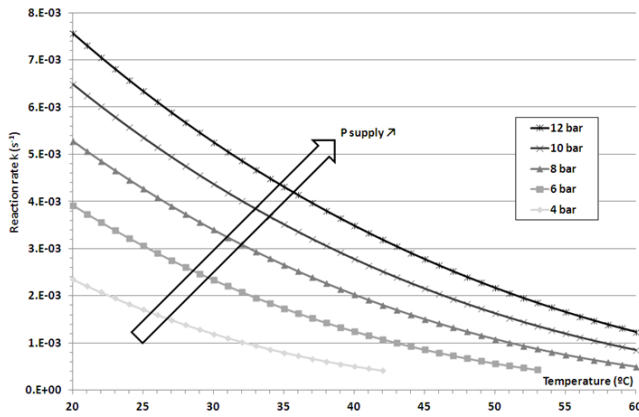


Figure 9. Reaction rate dependence on the temperature and pressure in the $\alpha+\beta$ phase

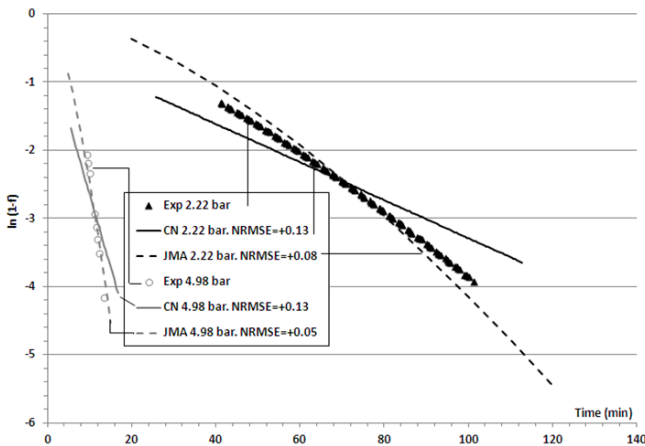


Figure 10. CN diffusion model adjustment at 22°C

Figure 5, only the $\alpha+\beta$ phase can be observed, whereas the rest of the applied pressures are sufficient to fully reach the β phase.

Several hydriding curves finish in the $\alpha+\beta$ phase, while other curves finish in the β phase region as indicated before in Figure 3.

Figure 5 and Figure 6 show the fitting of the JMA model with the measured absorption curves at 39°C and 43°C. As the hydrogen absorption in the α phase takes place very fast, the observed reacted fraction reveals mainly two different phase regions; the plateau (left) and the β phase (right). As may be inferred from Figures 5 and 6 and from the low NRMSE values, the nucleation and growth JMA model provides a very accurate fitting with the hydriding data, for both the $\alpha+\beta$ and the β phase.

Initially, the reaction order n was calculated by means of a linear regression analysis (Eq. 4) and values around $n_{\alpha+\beta}=1$ and $n_{\beta}=1.5$ were obtained indicating that the reaction order remained unchanged. The good agreement of the model adjustment has shown that the absorption process in the plateau region responds to a first order reaction rate (Eq.2), whereas the reaction order in the β phase is of around 1.5. These values are in coherence with the published literature [13] and reveal important information on the controlling processes.

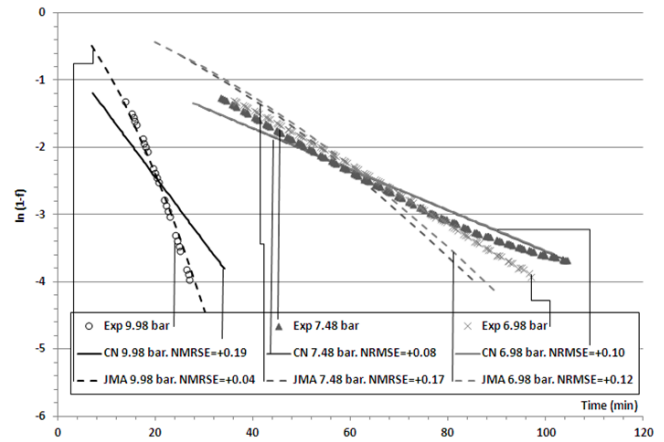


Figure 11. CN diffusion model adjustment at 57°C

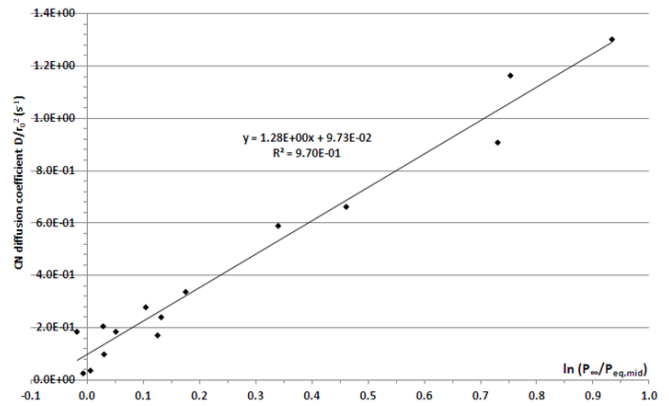


Figure 12. Diffusion coefficient dependence on the pressure in the β phase

The results indicate that the nucleation and growth of the hydride is the controlling mechanism in the $\alpha+\beta$ phase. In the β phase, the hydrogen diffusion through the hydride phase controls progressively the hydriding reaction. As the hydride layer grows, the diffusion distance increases and the hydrogen diffusion through the hydride phase becomes the rate controlling mechanism.

For instance, in Figure 5 the higher pressure (7.98 bar) presents a worse fitting than for the other measured pressures. The quality of the fitting is improved substantially by increasing the reaction order. In the plateau region, the NRMSE improves from -1.06 to -0.16 and in the β phase, the NRMSE improves from +0.08 to +0.0044.

The progressive change towards a diffusion controlled system is also clearly illustrated in Figure 6, where the reaction order $n_{\alpha+\beta}=1$ and $n_{\beta}=1.5$ provides good results at 4.5 bar and 5 bar, but at 9 bar a higher reaction order is required. For this higher pressure, the reaction rates $n_{\alpha+\beta}=1.83$ and $n_{\beta}=2.31$ provide the best agreement as shown by the visual fitting of the curves and by the low NRMSE values (-0.024 and +0.015 respectively).

The reaction rate constant k has been obtained for each isotherm and pressure with the data shown in Figures 5 and 6. One important aspect is to correlate the reaction rate constant with the temperature

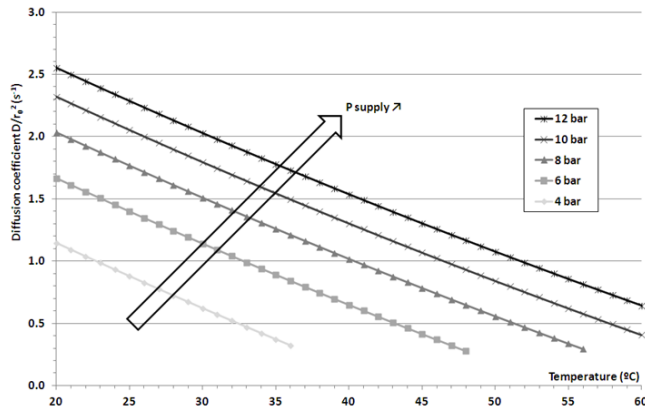


Figure 13. Diffusion coefficient dependence on the temperature and pressure

and pressure and hence understand the driving forces of the sorption process. For this purpose in Figures 7 and 8, the reaction rate constant has been correlated to the temperature and pressure conditions. In both the two-phase region and the β phase, the experimental results can be directly correlated to the function $\varphi(P,T)$ by means of the polynomial expression given in eq. (6). The obtained correlation coefficients for the $\alpha+\beta$ -phase region and β -phase region are $R^2_{\alpha+\beta}=0.968$; $R^2_{\beta}=0.982$, respectively.

As may be inferred from the scale of Figures 7 and 8, the reaction rate constant, k , is slower in the β -phase region than in the $\alpha+\beta$ -phase region. This aspect is in agreement with other authors [11].

Figure 9 represents the effect of the supply pressure and temperature on the reaction rate. The highest reaction rates are obtained with the highest tank pressure and the lowest temperature. For low temperatures, the effect of the supply pressure on the reaction rate is higher.

4.2. CN diffusion model

As the JMA model seems to indicate that the sorption reaction is diffusion controlled in the β phase, the CN diffusion model has been applied in the β phase in order to verify this hypothesis.

In Figures 10 and 11 the CN approach has been applied and compared with the sorption measurements. The results of the JMA model have also been plotted in order to allow for a comparison between both models.

The low NRMSE values indicate that the CN method reproduces accurately the experimental dynamics and is hereby an interesting tool for hydriding processes taking place in the β phase of the tested LaNi₅ alloy.

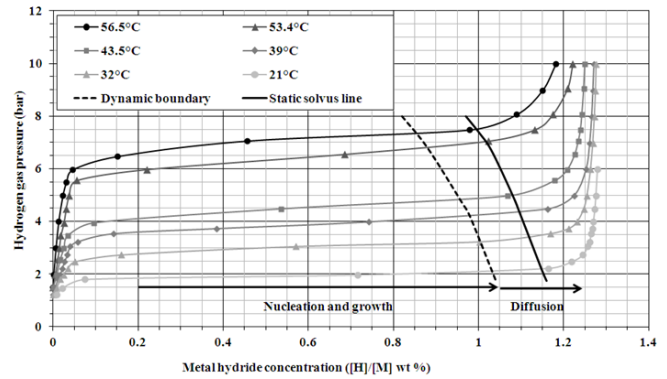


Figure 14. Static vs dynamic $(\alpha+\beta)\rightarrow\beta$ boundary

In Figure 10, the absorption curves at 22°C have been represented. The CN method can only be applied for diffusion-controlled mechanisms, in other words, in the β phase. At 22°C, only the applied pressures of 2.22 bar and 4.98 bar enable a full hydrogen absorption reaching the β phase. The lowest pressure which was tested for this isotherm was 1.97 bar, which corresponds to the middle of the plateau region and was hereby controlled by a nucleation and growth process.

The low NRMSE values which are given in Figures 10 and 11 show that the quality of the fitting with the CN method is similar to the JMA model.

As for the JMA model, the diffusion coefficient has been correlated in Figures 12 and 13 with the pressure and temperature. The fitting of the function $\varphi(P,T)$ in Eq. (9) provides a very good agreement, as shown by the high R^2 value of the fitting (0.972).

Table 2 shows the diffusion coefficient D_0 which is obtained applying the Eq. (9) to the experimental results. A close inspection of this table shows that the hydrogen diffusion coefficient varies from $1.5 \times 10^{-8} \text{ cm}^2 \text{ s}^{-1}$ to $9.7 \times 10^{-8} \text{ cm}^2 \text{ s}^{-1}$, depending on the average particle radius r_0 which is in the range from 4 to 10 μm , respectively. The values obtained by applying the CN method are in agreement with former publications [34-36].

In Figure 13, the diffusion coefficient has been illustrated as a function of the supply pressure and temperature. The higher diffusion coefficients are obtained for low temperatures and high supply pressures. For high temperatures or low supply pressures, the applied pressure is almost equal to the equilibrium pressure of the sample and thus a lower diffusion coefficient is obtained.

4.3. Dynamic behaviour

From the evolution of the reacted fraction (Figure 5 and 6), two different controlling mechanisms may be distinguished. The re-

Table 2. Comparison of present results with diffusion coefficients from the literature [30-32]

Authors and Reference	Material	Temperature (°C)	Diffusion coefficient ($\text{cm}^2 \text{ s}^{-1}$)
E. L. Cussler [31]	Hydrogen in nickel	85	$1.16 \cdot 10^{-8}$
Züttel [30]	Hydrogen in nickel	25	$3.12 \cdot 10^{-11}$
J. Han and J.-Y. Lee [32]	Hydrogen in LaNi ₅	25	$1.50 \cdot 10^{-8}$
Present work			
$r_0=4 \mu\text{m}$			$1.55 \cdot 10^{-8}$
$r_0=5 \mu\text{m}$	Hydrogen in LaNi ₅	25	$2.43 \cdot 10^{-8}$
$r_0=10 \mu\text{m}$			$9.73 \cdot 10^{-8}$

acted fraction where the hydriding reaction starts to become diffusion controlled corresponds to metal hydride concentrations range between 0.71% and 0.97%.

The resulting dynamic boundary region has been represented in Figure 14 and is compared with the hydrogen solubility line from the static P-C-T diagrams. The boundary regions have been obtained by connecting the different inflexion points for each isotherm.

Figure 14 clearly shows that the transition of the rate controlling mechanism takes place slightly to the left in comparison with the static solvus line. Thus, when adjusting the different kinetic models for each phase region, it is important to focus on delimiting the boundary regions from the dynamic behaviour and not from the static P-C-T diagrams. One possible explanation for this is that the hydrogen flow rate tends to increase the plateau slope [19], hence pushing the static solvus line to the left during dynamic absorption.

5. CONCLUSION

In this paper, the hydriding kinetics of a LaNi_5 alloy has been obtained. The kinetics has been characterized by means of the Johnson-Mehl-Avrami model and of the Crank-Nicholson diffusion model. The reaction rate constant and the hydrogen diffusion coefficient have been correlated accurately with the temperature and pressure, hereby providing a simple tool for the prediction of the absorption curves under different temperature and pressure conditions.

The change of the rate controlling step takes place below the static $(\alpha+\beta)\rightarrow\beta$ solvus line. The results seem to indicate that around 65% of the maximum storage capacity is reached within a nucleation and growth process, whereas the last 35% of the reaction is slower and is controlled by the diffusion of hydrogen through the growing hydride phase. These results show the importance of adjusting the kinetic models according to the dynamic regions and not to the phase regions from the static P-C-T diagrams.

6. ACKNOWLEDGEMENTS

The authors gratefully acknowledge Marc Linder from the Institut für Technische Thermodynamik des Deutschen Zentrums für Luft- und Raumfahrt (DLR) for his support.

REFERENCES

- [1] R. Janot, J.B. Eymery, J.M. Tarascon, *J. Power Sources*, 164, 496 (2007).
- [2] M. Linder, R. Kulenovic, *Int. J. Hydrogen Energy*, 36, 3215 (2011).
- [3] H. Dhaou, F. Askri, M. Ben Salah, A. Jemni, S.B. Nasrallah, J. Lamloumi, *Int. J. Hydrogen Energy*, 32, 576 (2007).
- [4] P. Muthukumar, A. Satheesh, M. Linder, R. Mertz, M. Groll, *Int. J. Hydrogen Energy*, 34, 7253 (2009).
- [5] O. Boser, *Journal J. Alloys Compd.*, 46, 91 (1976).
- [6] S. Tanaka, J.D. Clewley, T.B., Flanagan, *J. Alloys Compd.*, 56, 137 (1977).
- [7] M. Miyamoto, K. Yamaji, Y. Nakata, *J. Alloys Compd.*, 89, 111 (1983).
- [8] J. Bloch, *J. Alloys Compd.*, 312, 135 (2000).
- [9] E.H. Kisi, A. Gray, *J. Alloys Compd.*, 217, 112 (1995).
- [10] A. Inomata, H. Aoki, T. Miura, *J. Alloys Compd.*, 278, 103 (1998).
- [11] A. Leela Mohana Reddy, S. Ramaprabhu, *Int. J. Hydrogen Energy*, 31, 867 (2006).
- [12] G. Srinivas, V. Sankaranarayanan, S. Ramaprabhu, *Int. J. Hydrogen Energy*, 32, 2480 (2007).
- [13] G. Srinivas, V. Sankaranarayanan, S. Ramaprabhu, *J. Alloys Compd.*, 448, 159 (2008).
- [14] N. Mani, S. Ramaprabhu, *Int. J. Hydrogen Energy*, 30, 53 (2005).
- [15] J. Liu, X. Zhang, Q. Li, K.-C. Chou, K.-D. Xu, *Int. J. Hydrogen Energy*, 34, 1951 (2009).
- [16] Q. Li, K.-C. Chou, Q. Lin, L.-J. Jiang, F. Zhan, *Int. J. Hydrogen Energy*, 29, 1383 (2004).
- [17] Q. Li, L.-J. Jiang, K.-C. Chou, Q. Lin, F. Zhan, K.-D. Xu, X.-G. Lu, J.-Y. Zhang, *J. Alloys Compd.*, 399, 101 (2005).
- [18] J. Crank, *The Mathematics of Diffusion*, Oxford University Press, Oxford, Great Britain (1975).
- [19] E. Anil Kumar, M. Prakash Maiya, S. Srinivasa Murthy, *Int. J. Hydrogen Energy*, 32, 2382 (2007).
- [20] J. Payá, M. Linder, R. Mertz, J.M. Corberán, *Int. J. Hydrogen Energy*, 36, 920 (2011).
- [21] G. Sandrock, *J. Alloys Compd.*, 293, 877 (1999).
- [22] F. Dreisbach, H.W. Lösch, P. Harting, *Adsorption*, 8, 95 (2002).
- [23] J. Payá, M. Linder, E. Laurien, J.M. Corberán, *Int. J. Hydrogen Energy*, 34, 3173 (2009).
- [24] J. Payá, M. Linder, E. Laurien, J.M. Corberán, *J. Alloys Compd.*, 484, 190 (2009).
- [25] Y. Fukai, *The Metal-Hydrogen System*, 88 (1992).
- [26] J.-Y. Lee, C.N. Park, S.M. Pyun, *J. Alloys Compd.*, 89, 163 (1983).
- [27] Y. Ben-Eliyahu, M. Brill, M.H. Mintz, *J. Chem. Phys.*, 111, 6053 (1999).
- [28] R.A. Varin, T. Czujko, E.B. Wasmund, Z.S. Wronski, *J. Alloys Compd.*, 432, 217 (2007).
- [29] A. Jemni, S.B. Nasrallah, *Int. J. Hydrogen Energy*, 20, 43 (1995).
- [30] M.D. Mat, Y. Kaplan, *Int. J. Hydrogen Energy*, 26, 957 (2001).
- [31] M. Gambini, M. Manno, M. Vellini, *Int. J. Hydrogen Energy*, 33, 6178 (2008).
- [32] G. Mohan, M. Prakash Maiya, S. Srinivasa Murthy, *Int. J. Hydrogen Energy*, 32, 4978 (2007).
- [33] A. Demircan, M. Demiralp, Y. Kaplan, M.D. Mat, T.N. Veziroglu, *Int. J. Hydrogen Energy*, 30, 1437 (2005).
- [34] A. Züttel, *Metall-hydride Vorlesungsskript* (1988).
- [35] E.L. Cussler, *Mass transfer in fluid systems*, Cambridge University Press, University of Minnesota (1984).
- [36] J.I. Han, J.-Y. Lee, *Int. J. Hydrogen Energy*, 14, 181 (1989).